Exp. Theo. NANOTECHNOLOGY 10 (2026) 1255-1274 https://doi.org/10.56053/10.3.1255

Functional performance of carbon nanotube decorated nickel oxide as a smart nanoplatform for enhanced antibacterial and anticancer activity

Ali Hamandi[1,], Sahar. Al-Sammarraie[2], Hussein H. Abdulghani [1], Mustafa H. Amin[3], Hind M. Ahmed[1], Sadeer M. Majeed[1], Majid S. Jabir[1]*

[1]College of Applied Sciences, University of Technology, Baghdad, Iraq
[2]Applied Sciences Research Unit, College of Applied Sciences, University of Technology, Baghdad, Iraq
[3]Institute of Laser for Postgraduate Studies, University of Baghdad, Baghdad, Iraq
[*]) Email: ali.s.naseef@uotechnology.edu.iq

Received 15/3/2026, *Received in revised form* 23/5/2026, *Accepted* 18/6/2026, *Published* 15/7/2026

This work discusses the synthesis and characterization of NiO NPs and NiO/MWCNT nanocomposites (ratio 1:1 molar) via a sol-gel method, with an emphasis on improved biomedical applications. The fabrication of extraordinarily crystalline face-centered cubic NiO is verified through X-ray diffraction (XRD), and the characteristic (002) demonstrates the successful integration of MWCNTs. Fourier transform infrared (FTIR) spectroscopy indicate a significant interfacial coupling, as demonstrated by Ni-O-C bonding, which prove that MWCNTs are well incorporated into the NiO matrix. UV-Vis spectroscopy revealed a red shift in the absorption edge and a reduction in the band gap from 3.5 eV (NiO) to 3.1 eV (nanocomposite), which indicate an improvement electronic interactions and charge transfer. Photoluminescence (PL) research revealed a significant quenching, indicating a reduced in the electron-hole recombination and increased charge separation. Field emission scanning electron microscopy (FE-SEM) revealed a well dispersed NiO nanoparticles which anchored onto the nanotube network, that leads to reduce the particle size and increased the surface area. Due to synergistic actions such membrane rupture and reactive oxygen species production, the nanocomposite demonstrated improved antibacterial activity against both Gram-positive and Gram-negative pathogens. Due to synergistic actions such membrane rupture and reactive oxygen species production, the nanocomposite demonstrated improved antibacterial activity against both Gram-positive and Gram-negative pathogens. Furthermore, an increasement in the ROS generation and apoptosis induction are linked to increased

cytotoxicity against A549 cancer cells. These results demonstrate a great potential of the nanocomposites for antibacterial and biological uses.

Keywords: NiO/MWCNT nanocomposites; Sol–gel; Band gap; Reactive oxygen species (ROS); Antibacterial.

1. INTRODUCTION

The structural, physical, morphological, electrical, and practical properties of the fabricated nanocomposite are greatly enhanced by the incorporation of multiwalled carbon nanotubes (MWCNTs) to the Nickel oxide (NiO) matrix. due to their high surface area, mechanical properties, and excellent electrical conductivity. they considered an excellent dispersion agent and conductive scaffold for NiO nanostructures the functional groups of oxygen that located MWCNTs surface will interact with the Ni^{2+} ions during the sol-gel processes, which lead to uniform deposition of NiO nanostructures across nanotube walls. Improved dispersion, stability, and interfacial contact between the NiO and MWCNT phases result from this process's successful suppression of particle agglomeration [1,2]. The electrical composition and charge transfer performance of the composite are significantly modified by the powerful interfacial bonding between NiO and MWCNTs, mainly through Ni–O–C connections. This interaction reduces recombination of the charge carriers yet improving the general electrical conductivity by allowing efficient electron transport through the heterojunction. this Rapid charge flow inside the composite can be achieved by the creation of this conductive network, which is particularly beneficial in catalytic, sensing, and antibacterial applications [3,4]. NiO nanostructures are evenly fixed on MWCNTs surfaces, creating a three-dimensional interconnected network that improves surface roughness and porosity, according to field-emission scanning electron microscopy (FE-SEM) results from earlier research [5]. Catalytic and antibacterial activities are improved as a result of the increased surface area, which improves adsorption and contact between active sites and bacterial cells. Furthermore, the hybrid structure preserves mechanical strength and is more resistant to aggregation than pure NiO. Optical investigation confirms the mutually beneficial interaction of NiO with MWCNTs. This incorporation of MWCNTs induces a noticeable reduction in the optical band gap energy of NiO, will lead to from the π–π conjugated electronic structure of MWCNTs, which facilitates charge delocalization and light absorption in the visible region. usually the pure NiO exhibits a direct band gap in the range of 3.4–3.6 eV, whereas integration with MWCNTs decreases the effective band gap to approximately 3.02–2.6 eV, depending on synthesis parameters and MWCNTs loading [6–8]. The narrowing in the band gap can not only improves the visible light usage, but also it can stimulate the production of oxygen species that are reactive (ROS), which contributes to better photocatalytic and biological efficiency.

This combination structural and electrical interaction is the cause for NiO/MWCNTs nanocomposites' increased antibacterial effectiveness. The conductive MWCNTs network increases electron transport, inhibiting recombination of photogenerated charge carriers in NiO and boosting ROS generation, which damages bacterial cell membranes. MWCNTs' large surface area enables for close contact with bacterial cells, resulting in mechanical disruption and increased diffusion of Ni^{2+}. As a result, this hybrid system outperforms the pure NiO in terms of the antibacterial efficacy, and highlighting the high potential of NiO/MWCNT nanocomposites in the biomedical and the environmental disinfection applications. In addition to antibacterial activity, nanocomposites have interesting anticancer properties. The increased production of ROS and greater cellular contact promote oxidative stress-induced apoptosis in cancer cells. Furthermore, the conductive feature of MWCNTs leads to stimulates intracellular electron

transport, which increases ROS generation and cytotoxicity. Nanomaterials can make a great alternative for biological applications due to their synergistic activities, particularly in cancer therapy [9,10-14].

In summary, the incorporating of MWCNTs into the NiO matrices can enhance particle dispersion, electrical conductivity, band gap inhibition, and antibacterial activity. These results highlight the essential function of MWCNTs in controlling the functional and physical characteristics of NiO-based nanostructures, which renders them interesting candidates for multifunctional nanomaterial applications. In this work, pure NiO and NiO/MWCNTs with a particular molar ratio of 1:1 NiO:MWCNTs are effectively synthesized utilizing the Sol-Gel technique. the XRD, FTIR, UV-Vis, PL analysis, and FE-SEM are used to analyze the structural, optical, and morphological properties. Additionally, the cytotoxic and ROS-generating impacts on cancer cells, as well as the antibacterial activity towards Gram-positive and Gram-negative bacteria, are investigated. The results show that the efficiency of NiO can greatly improve by adding MWCNTs demonstrating the possibility of NiO/MWCNTs nanocomposites for superior biomedical and environmental applications.

2. EXPERIMENTAL

2.1 Materials

All reagents employed in this study are of analytical grade and used without further purification. Nickel nitrate hexahydrate ($Ni(NO_3)_2 \cdot 6H_2O$) and ammonium hydroxide (NH_4OH) are procured from Aladdin Chemical Co. (China), while sodium hydroxide (NaOH) is obtained from Chemical Reagent Com (China). Multi-walled carbon nanotubes (MWCNTs) with a reported purity of ~90% and diameters ranging from 8 to 15 nm are purchased from Grafton (USA). Deionized (DI) water is used throughout all synthesis procedures under ambient laboratory conditions.

2.2 Synthesis of pure NiO nanostructures and NiO/MWCNTs nanocomposites

Pure NiO and NiO/MWCNTs nanocomposites are prepared using sol-gel method, which consider one of the most flexible and popular technique for meatal oxide nano materials fabrication with a controlled shape and high purity [15,16]. For pure NiO preparation 50 mL of 0.5 M nickel nitrate hexahydrate ($Ni(NO_3)_2 \cdot 6H_2O$) solution is incorporated with 100 ml of 2M ammonium hydroxide (NH_4OH) solution dropwise on a magnetic stirrer at 90°C for 4 hours. The obtained sol is aged at room temperature for 24 hours, to ensure gel formation and structural stability. After centrifuge a light-green suspension is obtained, the collected precipitate is dried at 90 °C for 2 hours and then calcined for 2 hours at 450 °C to obtain pure NiO nanostructures.

For the synthesis of the NiO/MWCNTs nanocomposite, a 1:1 molar ratio of NiO to multiwalled carbon nanotubes (MWCNTs) is used. NiO and MWCNTs nanoparticles is dispersed in 100 mL of deionized (DI) water under magnetic stirring to form solution (1). Separately, 8 mmol of sodium hydroxide (NaOH) is dissolved in 50 mL of DI water to form solution (2). Solution (2) is then added dropwise to solution (1) containing dispersed MWCNTs under continuous stirring at room temperature. The resulting precipitate is collected by centrifugation, thoroughly ished several times with DI water, and dried in an oven at 90 °C for 2 hours. The final product is calcined at 450 °C for 2 hours to obtain the NiO/MWCNTs nanocomposite with homogeneous particle distribution and strong interfacial bonding between NiO and MWCNTs.

2.3 Defining characteristics

The crystalline phase and structural characteristics of the synthesized nickel oxide (NiO) and NiO/MWCNTs nanocomposites are analyzed using an XRD diffractometer (XRD PW1730, Philips, Netherlands), with CuK radiation (λ = 1.542Å), the data that is acquired fell between the range of 10˚ to 70˚, The optical properties and band gaps are measured using UV−visible spectroscopy (Sgimadzu UV-1900 ,spectrophotometer, Jaban).FTIR spectrum (Thermo Nicolet, USA)) is employed to analyze the boundary construction of the resulting samples. The samples are mixed with KBr powder and pressed to form the semitransparent pellets in the 4000–400 cm^{-1} range. Photoluminescence (PL) spectroscopy is performed using excitation wavelength of about 325 nm (Cary Eclipse Fluorescence Spectrometer, Agilent Co model, America) at room temperature to analyze the emission wavelengths of NiO , NiO/MWCNTs in the range of 200−900nm. Filed emission scanning electron microscope images (FE-SEM, TESCAN, MIRA3, Day Petronic Company/Tehran/Iran) of pure NiO, NiO/ MWCNTs nanocomposite samples are captured to study their morphology. Besides, EDS stands for energy-dispersive X-ray spectroscopy is conducted during FE-SEM measurements as a relatively simple but powerful technique for the elemental analysis.

2.4 Antibactreal acivity

The antibacterial activity of prepared nanoparticles samples (NiO and NiO/MWCNTs) nanocomposites is tested using the agar well diffusion method [17] against gram- positive bacteria, including *S. aureus* and gram-negative bacteria including *E. coli*. The bacterial samples are inoculated in 6 mm diameter wells of petri dish. The final concentration (0,31.25, 62.5, 125 and 250 μg/ml) of pure NiO and NiO/MWCNTs nanocomposites are added into the wells. The plates are incubated overnight at 37ºC before measuring the inhibition zone diameter.

2.5 MTT assay

Using the MTT assay, the cytotoxicity of pure NiO and NiO/MWCNTs nanocomposites is examined. A549 cells are cultivated overnight and then seeded at a density of $1x10^4$ cells per well on to 96-well plates. Following, the removal of the growth media and its replacement with 200 μL of fresh medium with different concentration for 72h [18]. The cells are treated for 3 hours with MTT solution consisting 2 milligrams per milliliter (Invitrogen, Carlsbad, CA) after being with PBS. Each well is then filled with 100μL of DMSO after the solution had been emptied away. The absorbance of each sample at wavelength of 492 nm is measured using a microplate reader. The formula used to calculate the percentage of cytotoxicity, or the rate of inhibiting of cell growth, is displayed:

$$\text{Cytotoxicity} = (A-B)/B \quad (1)$$

where A exhibits the optical density of control and B exhibits the optical density of product [19].

2.6 ROS generation assay

A flow cytometry assay is used to quantify the generation of ROS in cells. Each well is seeded with $1x10^6$ A549 cells. The cells are treated with pure NiO, and NiO/MWCNTs nanocomposites for 12 hours after being incubated overnight. The modified medium is then incubated for a further half hour in the dark with a ROS probe (DCFH-DA) at a concentration of 20 μM. A flow cytometer is used to quantify the cells fluorescence intensity.

2.7 Statistical analysis

Three separate experiments produced the final data. Data are shown as mean ± SD. Graph Pad Prism (7) is used to perform the statistical analysis by applied of one-way ANOVA analysis of variance. LSD is used to evaluate the differences between means: $p \leq 0.05$ proved to be significant. $P^{*} \leq 0.05$, $p^{**} \leq 0.01$, $p^{***} \leq 0.000139$.

3. RESULTS AND DISCUSSION

3.1 X-ray diffraction (XRD) analysis

The crystal structure and phase formation of pure NiO and NiO/MWCNTs nanocomposites are analyzed, respectively by X-ray diffraction (XRD), as shown in Figure (1). The XRD pattern of pure NiO nanostructure (blue curve) exhibits characteristic diffraction peaks at 2θ= 37.2°, 43.3°, 62.8°, 75.4°, and 79.5°, corresponding to the (111), (200), (220), (311), and (222) planes, respectively, of face-centered cubic NiO (FCC) in agreement with JCPDS card no. 47-1049. These peaks confirm the formation of highly crystalline NiO nanostructure. This high crystallinity is consistent with previous reports on sol-gel synthesized NiO [18,20]. In Figure 1 (black curve), the XRD pattern of the NiO /MWCNTs nanocomposite reveals additional peak at 2θ= 25.2°, which are assigned to the (002) plane of multi-walled carbon nanotubes (MWCNTs), in accordance with JCPDS card no. 0646. The appearance of these peaks indicates that the MWCNTs retain their graphitic structure and are effectively integrated within the NiO/MWCNTs matrix. Overall, the XRD analysis proves the crystalline nature and phase purity of all samples, it also verifies that MWCNTs are successfully incorporated into the NiO matrix with no interfere in the NiO the face-centered cubic structure. Moreover, the peaks intensity of NiO are noticeably lower than the intensity of the pure NiO. The average crystallite size of NiO and NiO/MWCNTs is calculated by using the Scherrer equation [21]:

$$D = \frac{K\lambda}{\beta cos\theta} \quad (1)$$

where D is the crystallite size in nanometers, K is the shape factor (typically 0.9), λ is the X-ray wavelength (0.15406 nm for Cu Kα radiation), β is the full width at half maximum (FWHM) of the peak in radians, and θ is the Bragg angle. The analysis is performed on the three most intense diffraction peaks observed in the X-ray diffraction (XRD) pattern. The 2θ positions, corresponding Miller indices (hkl), and the calculated crystallite sizes for these peaks are presented in Table 1.

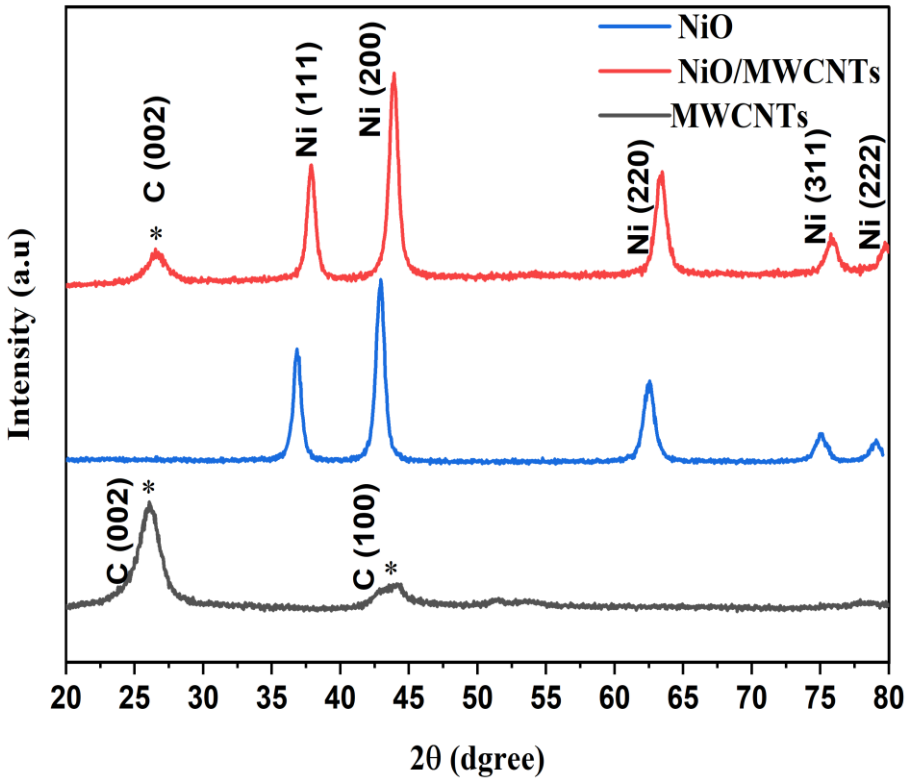

Figure 1 XRD pattern of pure NiO nanostructure and NiO/ MWCNTs nanocomposites at specific molar ratio (1:1) by sol gel method.

Table 1 XRD parameters analysis of pure NiO and NiO/MWCNTs nanocomposite at molar ratio (1:1).

Materials	2θ (deg)	hkl	FWHM (rad)	Grain size (nm)	d (Å)	a (Å)	c (Å)
NiO before added MWCNTs	37.3°	111	0.01869	7.83	2.406	2.410	2.410
	43.3°	200	0.0135	11.38	2.084		
	62.9°	220	0.015882	10.25	1.475		
NiO/MWCNTs nanocomposite	37.2°	111	0.0187	7.81	2.410	-	-
	43.2°	200	0.01309	11	2.087		
	62.7°	220	0.01589	10.22	1.476		

According to the findings in Table 1, the calculated crystallite size of pure NiO and NiO/MWCNTs nanocomposites at molar ratio 1:1 of NiO:MWCNTs by using the Scherrer equation are in the range of 7.81–11.38 nm and 7.83–11.0 nm, respectively. Data show that adding MWCNTs to the pure NiO leads to a slight reduction in average crystallite size. This demonstrates an enhancement in the crystallization of NiO. The role of carbon nanotubes as growth inhibitors, which limit crystal development and lessen particle aggregation, may be responsible for the little drop in NiO crystallite size following the addition

of MWCNTs. Smaller NiO crystallites and a modest widening of the diffraction peaks are the results of the presence of MWCNTs, which also supply nucleation sites and prevent grain coarsening. [22-25].

3.2 Fourier transform infrared (FTIR) spectroscopy analysis

Figure 2 (a,b) shows the FTIR spectra of pure NiO and the NiO/MWCNTs nanocomposite in the 500–4000 cm^{-1} wavenumber range. The formation of crystallized NiO with cubic phase structure is demonstrated by the absorption band seen at around 435 cm^{-1} for the pure NiO sample, which matched the stretching vibration of the Ni–O bond.

bands around 815 cm^{-1} (C–H) and 1373 cm^{-1} (C=O or O–H bending) may be attributed to the adsorbed carbon-containing molecules or remaining organic substances from the precursor or solvent employed during production. The broad absorption at 3453 cm^{-1} is caused by the O–H stretching vibrations of surface hydroxyl groups or interlayer water molecules, while the weak band around 1635 cm^{-1} is due to the bending vibration of the O-H group physically adsorbed water molecules on the surface. These characteristics imply the existence of surface hydroxylation and a tiny amount of moisture maintained inside the NiO lattice, which is common of NiO nanostructures formed through wet chemical processes. [27,23]. In comparison to pure NiO, the spectrum of the NiO/MWCNTs nanocomposite at molar ratio 1:1 NiO:MWCNTs in Figure 2 (b) shows many shifted bands. Compared to the pure NiO sample, the Ni-O vibration is slightly shifted to a higher wavenumber at 566 cm^{-1}. this change implies that significant surface interaction between NiO and the functional groups of the MWCNTs have altered the local chemical environment of Ni^{2+} ions. The bands at 1044 cm^{-1}, 1563 cm^{-1}, and 1703 cm^{-1} are attributed to C–O, C=C, and C=O stretching vibrations, respectively. These bands are indicative of the carbon nanotubes' graphitic structure and oxygen-containing functional groups. The presence of these peaks indicates that MWCNTs are successfully integrated into NiO matrix and that their surface function is retained in the nanocomposite [22,26]. The Ni–O band's upward shift from 435 cm^{-1} to 566 cm^{-1} suggests that the Ni–O bonding in the composite become somewhat stronger. This could be due to from electron transfer between Ni^{2+} and the π-electron system of CNTs, electron system, which could cause lattice strain or partial charge redistribution at the NiO/MWCNTs interface [24].

Moreover, the presence of C=O and C–O vibrations suggests that oxygen group on CNT interfaces act as positions of anchoring for Ni^{2+} ions throughout nucleation, generating strong Ni–O–C connections. Increased crystallinity and minor variations in lattice vibration frequencies are the outcomes of these linkages, which also improve heat conduction during computation and increase electron mobility across the interface and adhesion between NiO and MWCNTs [23]. FTIR spectra are frequently used to validate the existence of NiO and carbon nanotube structure in the composite.

The shifts in Ni-O vibrations, along with the emergence of carbon-related functional bands, clearly demonstrate the formation of interfacial bonding and chemical coupling between NiO nanostructures and MWCNTs. Such interactions enhance structural ordering and electronic communication within the hybrid material, which in turn improve its physicochemical stability and conductivity-an observation consistent with other recent studies on NiO/MWCNTs hybrid systems.

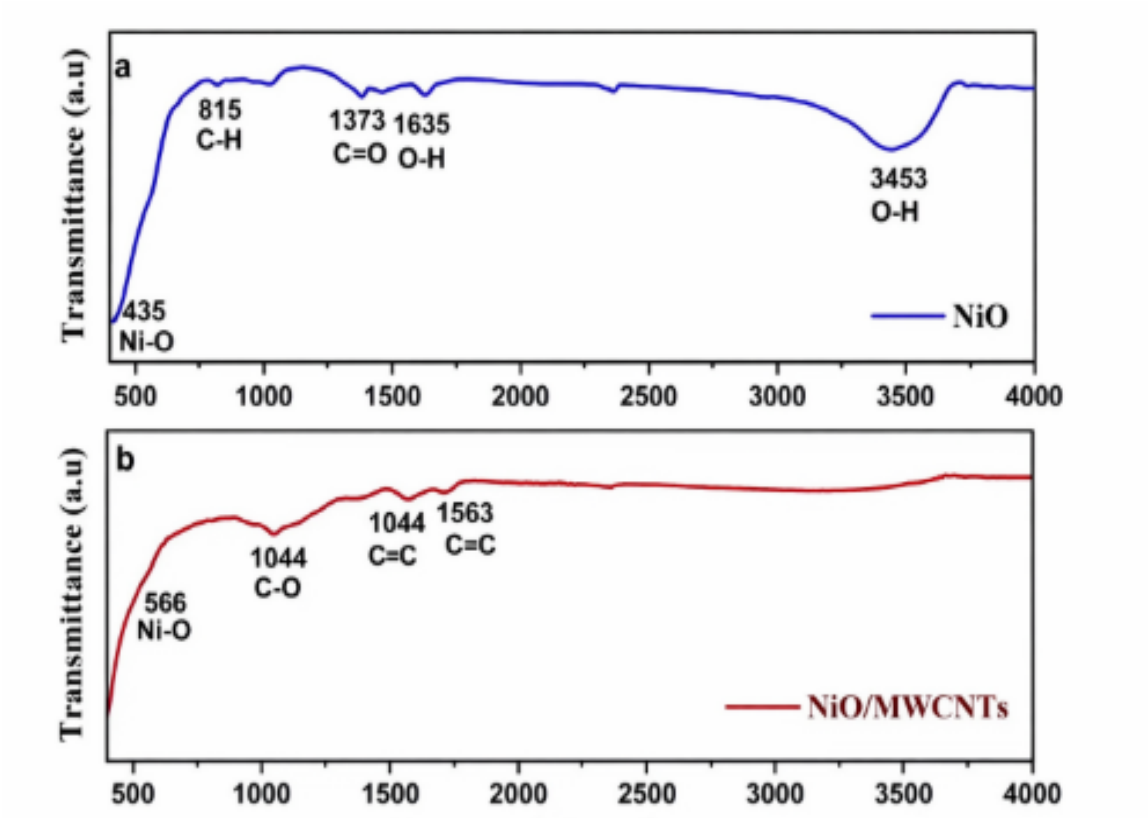

Figure 2 Comparison of FTIR spectra for: a) pure NiO and b) NiO /MWCNTs nanocomposite at molar ratio 1:1 NiO:MWCNTs.

3.3 UV-vis spectrophotometry analysis

The optical behavior of the synthesized pure NiO nanostructures and the NiO/MWCNTs nanocomposite at molar ratio 1:1 NiO:MWCNTs is further examined through the UV–Vis absorption spectra shown in Figures 3 (a ,b), respectively, in the wavelength range of 300–800 nm. Pure NiO displays a well-defined absorption edge at around 390 nm, indicative of its wide band-gap semiconducting nature and high degree of crystallinity. The gradual reduction in absorbance toward the visible region, along with the presence of a slight Urbach tail, suggests a relatively low density of defect states-consistent with the sharp and distinct XRD patterns previously reported for NiO [28,29].

In comparison, the spectrum of the NiO/MWCNTs nanocomposite Figure 3(b) exhibits a noticeable red shift of the absorption edge to approximately 403 nm, together with an enhancement in visible-light absorption, now this effect is caused by surface electron contact between NiO and MWCNTs, which result in higher localized state at the band edge and improves charge transfer processes. Recent study has also revealed that the synergistis interaction between NiO and conductive carbon nanotubes improve light harvesting capacity and modifies optical properties [30,32]. Band-gap energies are calculated using Origin software from the linear region of the $(\alpha h\nu)^2$ versus photon energy ($h\nu$), using the equation:

$$E_g = -\frac{interception}{slope} \quad (2)$$

where the interception is the extended linear fit on the photon energy axis, and the slope represents is the gradient of the linear segment. Now. These finding support the gradual shrinking of the band gap with each additional component. the optical band gaps of the samples are determined from the Tauc plots presented in Figure 3 (c,d). For the pure NiO, the band gap is calculated using the Tauc plots which presented in Figure 3 (c and d). The NiO is found to be 3.4 Ev, which is correspond to its fast absorption and improved crystallinity, as validated by XRD. The band gap in the NiO/MWCNTs nanocomposite reduced to be 3.1eV.

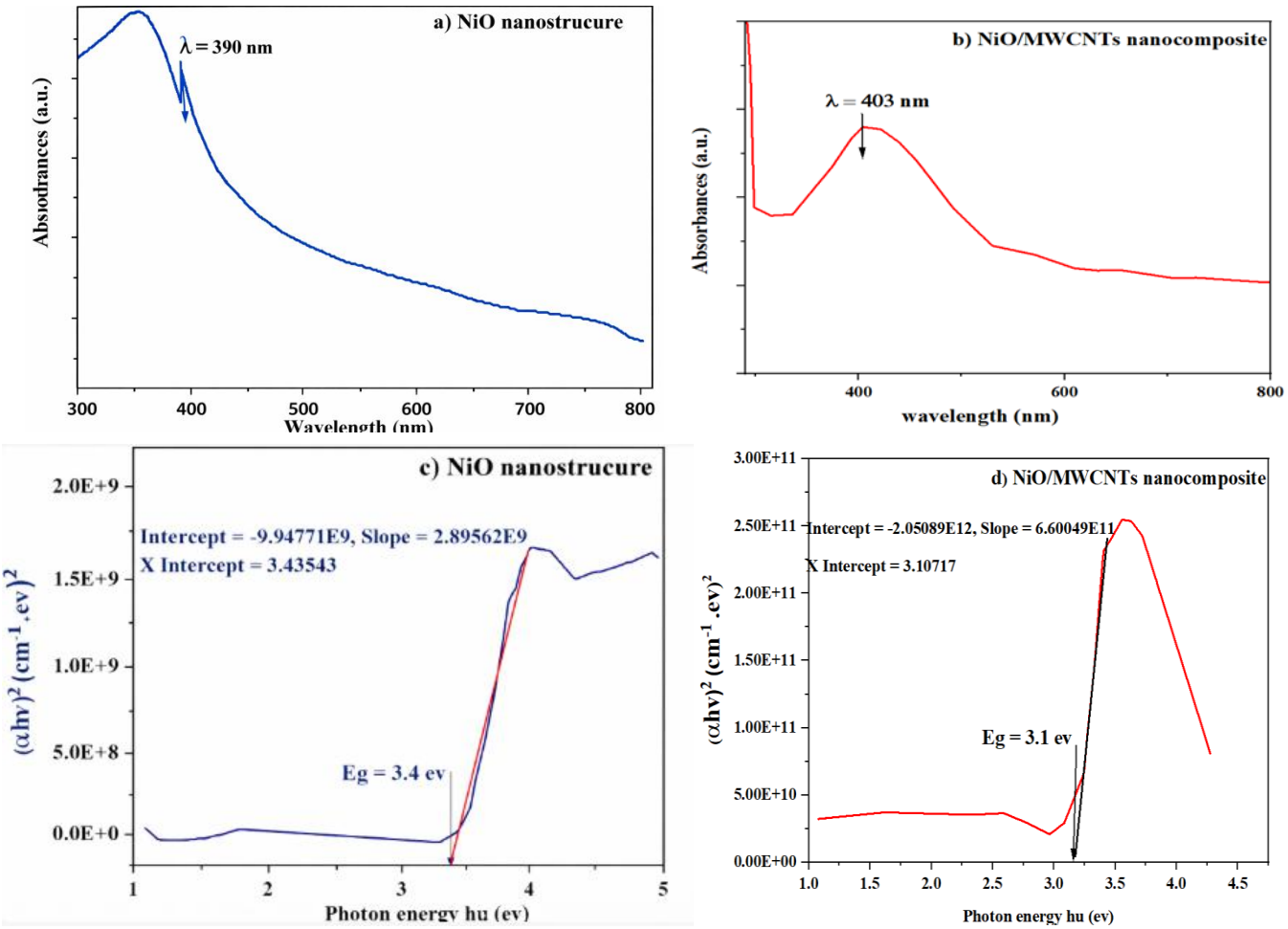

Figure 3 UV-visible absorption spectra of a) pure NiO, NiO/MWCNTs nanocomposites at molar ratio 1:1 of NiO: MWCNTs and Tauc plots for (c) NiO nanostrucure and (d) NiO /MWCNTs nanocomposites at molar ratio 1:1 of NiO: MWCNTs by sol-gel method.

3.4 Photoluminescence (PL) analysis

Figure 4 illustrates the photoluminescence (PL) spectra of pure NiO and the NiO/MWCNTs nanocomposite at a molar ratio (1:1). the PL spectrum of pure NiO indicate two emission peaks at 413 and 457 nm. The initial peak is due to near band edge emission caused by radiative recombination of electron in the conduction band with holes in valance band, where the second peak is caused by defect-associated recombination linking oxygen vacancies and nickel intermediates [33,34]. However, the NiO/MWCNTs nanocomposite exhibits a distinct peak shift and a considerable decrease in PL intensity.

The near band Edge emission is shifted towards longer wavelengths, while defect associated emission is seen at 591 nm, suggesting the formation of interface defect state and intense electronic interaction within NiO and MWCNTs. The intense reduction in PL indicate excellent separation of electron hole pairs produced by photons and reduced non-radiative recombination as result of fast charge transmission from Ni Oto MWCNTs, which serve as efficient charge transportation channels. These findings demonstrate that MWCNT inclusion considerably enhance charge extraction and lower recombination losses [35,36].

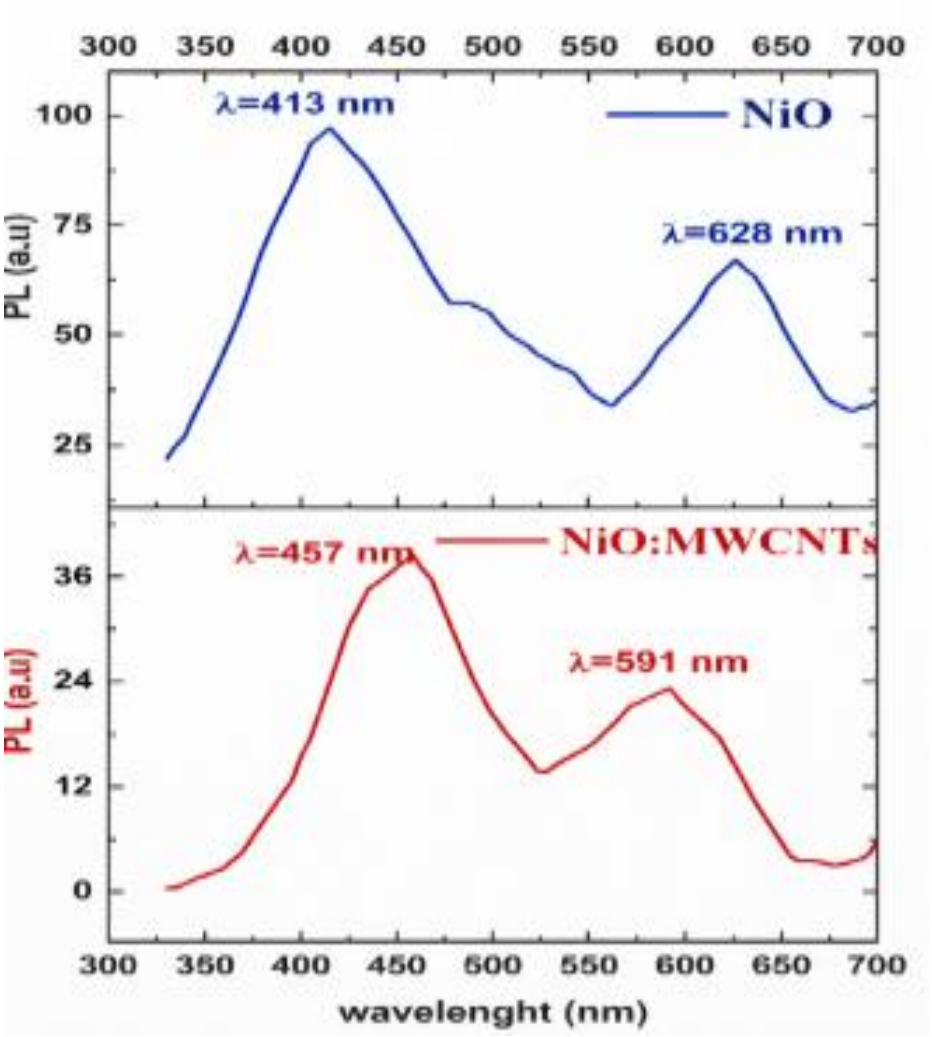

Figure 4 PL spectrum of the pure NiO nanostructure and NiO/MWCNTs nanocomposite at molar ratio 1:1 NiO:MWCNTs by sol-gel method.

3.5 Field emission-scanning electron microscopy (FE-SEM)

Figure 5 (a,b,c,d) shows the surface morphologies of pure NiO and NiO/MWCNTs nanocomposite at a molar ratio of 1:1. Pure NiO has a highly agglomerated morphology made up of plate like nanosheets with uneven staks and tight packing pattern as seen in Figure (a,b). Because of their high surface energy ans strong inter-particles interaction, NiO nanostructures have a strong tendency to aggregate during nanosheet during synthesis, as seen by this tight microstructure. The formation of cluster nanosheet

assemblies is supported by fast nucleation and uncontrolled crystal growth in NiO formed by precipitation or sol-gel techniques, as has been extensively reported [27].

However, Figure 5(c,d) shows the FE-SEM of the NiO/MWCNTs nanocomposite. The structure of the Figure is noticeably different and more open. NiO nanostructures are evenly distributed and attached onto aa network of linked MWCNTs in the FE-SEM micrograph. In order to efficiently separate NiO domains and restrict direct particle-particle interaction, the MWCNTs emerge as long, entangled tubular structures that create constant framework. During synthesis, the incorporation of MWCNTs serve as a growth control environment and physical restriction, allowing more consistent particle dispersion and limiting extreme growth of grains and aggregation.

The dense and relatively uniform morphology observed for pure NiO is in good agreement with the previously discussed XRD results, which confirmed the formation of a single-phase, highly crystalline NiO structure. Although the average crystallite size estimated from XRD lies in the nanoscale range (7–11 nm), the FE-SEM image and particle size distribution reveal that these primary crystallites tend to coalesce into larger agglomerated particles [28].

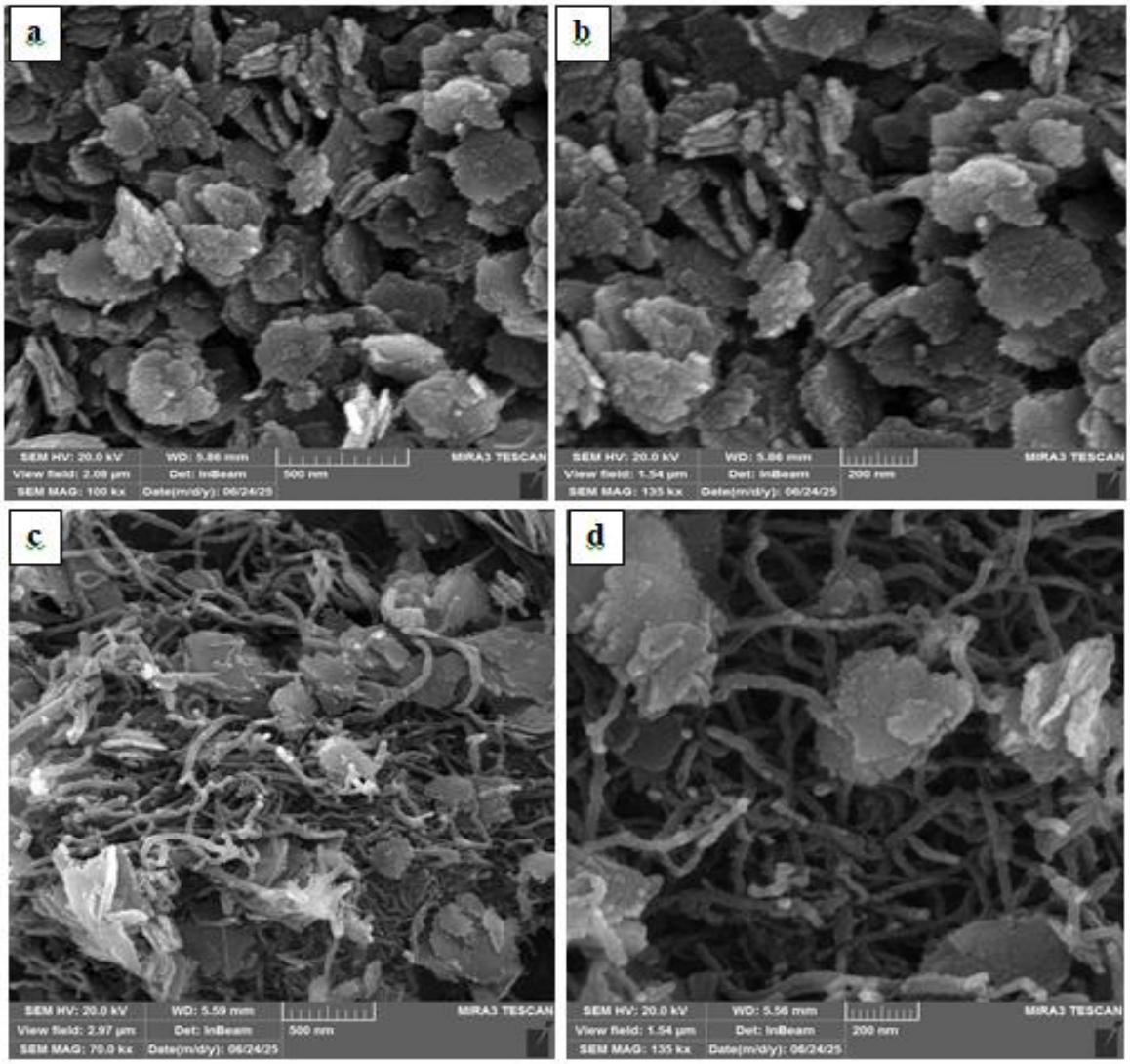

Figure 5 FE-SEM images of a,b) pure NiO nanostructure c,d) NiO/MWCNTs nanocomposite at molar ratio 1:1 NiO:MWCNTs at various magnified scale bar = 500 nm, 200 nm.

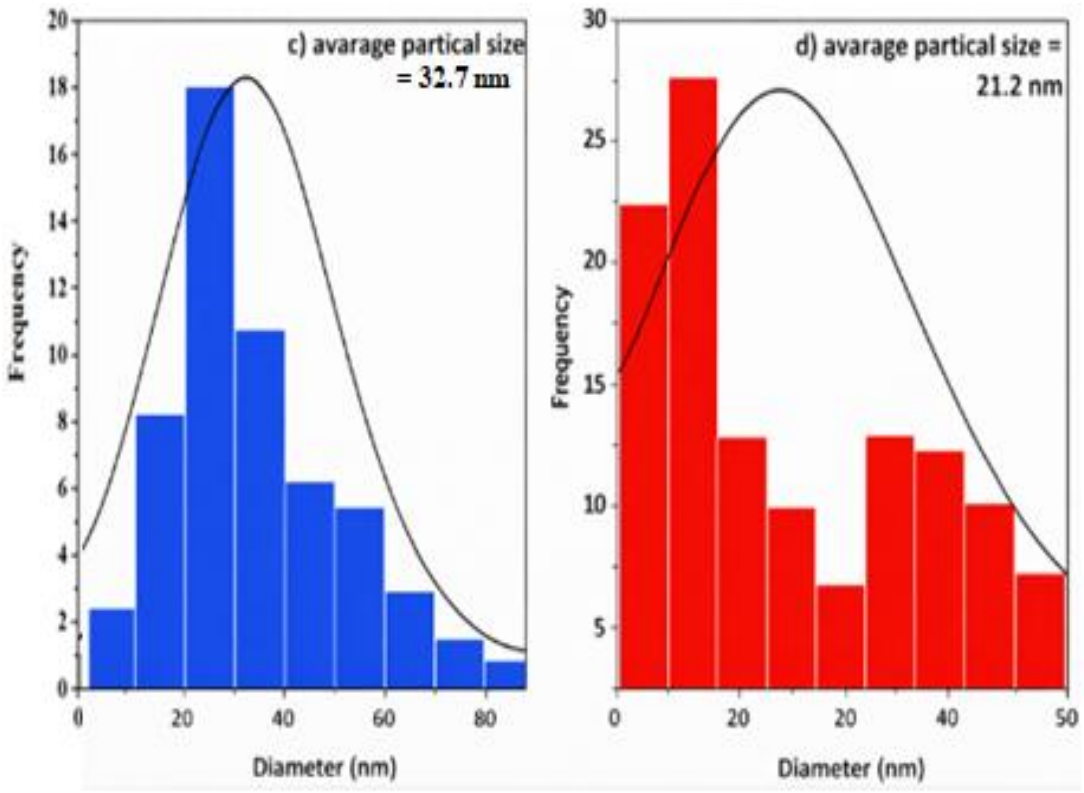

Figure 6 Average particle size of a) pure NiO nanostructure b) NiO/MWCNTs nanocomposite at molar ratio 1:1 NiO:MWCNTs**.**

The particle size distribution histograms created with the image J software, as seen in Figure 6(a,b), further highlight this morphological change. With an average particle diameter of around 32.7 nm, pure NiO has awide size variation that suggest significant growth of particles and aggregation during synthesis. The NiO/MWCNTs nanocomposite, on the other hand, has a much smaller size dispersion and smaller average particle size shows how well MWCNTs function as physical barriers that limit grain development and nucleation substrate [37-39].

Figure 7(a,b) shows the EDX spectra of pure NiO and the NiO/MWCNTs nanocomposite, respectively. The synthesis of chemically pure NiO with no apparent impurities is confirmed by the observation of only nickel (Ni) and oxygen (O). In the NiO/MWCNTs nanocomposite, Ni and O are preserved, however a strong carbon (C) signal develops, showing that MWCNTs are successfully incorporated into the NiO matrix. The high carbon concentration indicates the presence of the nanotube network, providing direct proof of the composite structure while maintaining NiO's chemical identity.

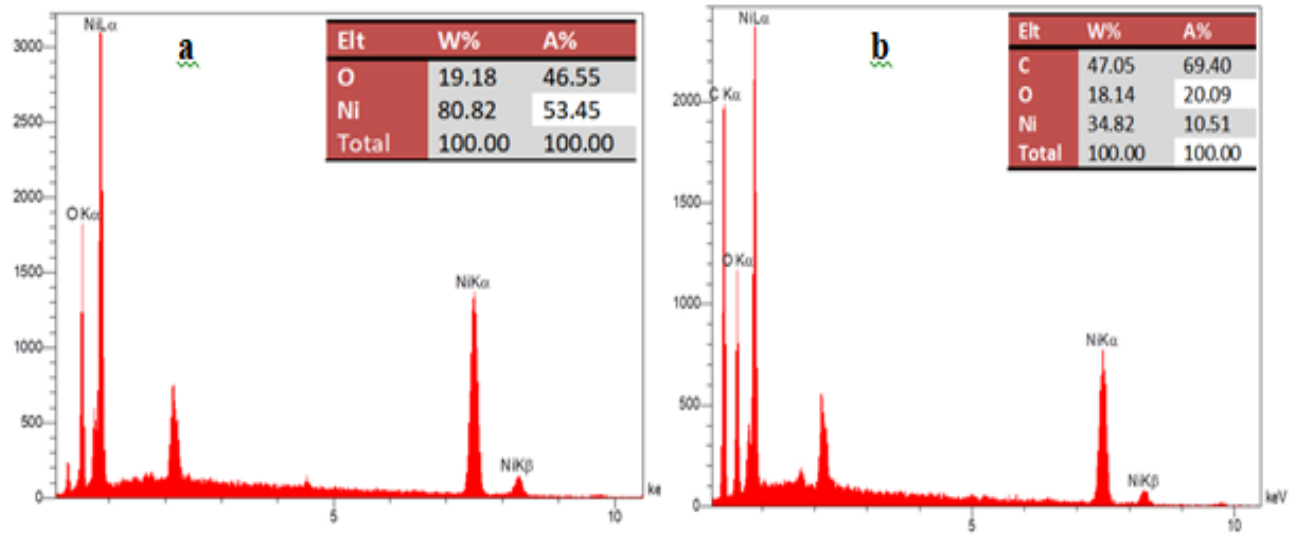

Figure 7 EDX spectrum of the a) pure NiO nanostructure and b) NiO/MWCNTs nanocomposite at molar ratio 1:1 of NiO: MWCNTs.

3.6 Antibacterial activity

The antibacterial activity of NiO NPs and NiO\MWCNTs nanocomposites against *S. aureus* is mainly attributed to physicochemical interactions between the nanomaterials and the bacterial cell membrane as shown in Figure 8, shows that the inhibition zone produced by NiO/MWCNTs nanocomposites is consistently larger than that of NiO at all tested concentrations. The NiO NPs can generate reactive oxygen species (ROS) such as superoxide (O_2^-) and hydroxyl radicals (•OH) on their surface. These ROS induce oxidative stress, which damages cellular lipids, proteins, and DNA. In addition, partial dissolution of NiO can release Ni^{2+} ions, which interfere with enzyme activity and disrupt metabolic pathways. Because *S. aureus* is a Gram-positive bacterium with a thick peptidoglycan layer, nanoparticles typically act by attaching to the cell wall, increasing membrane permeability and eventually causing leakage of intracellular components.

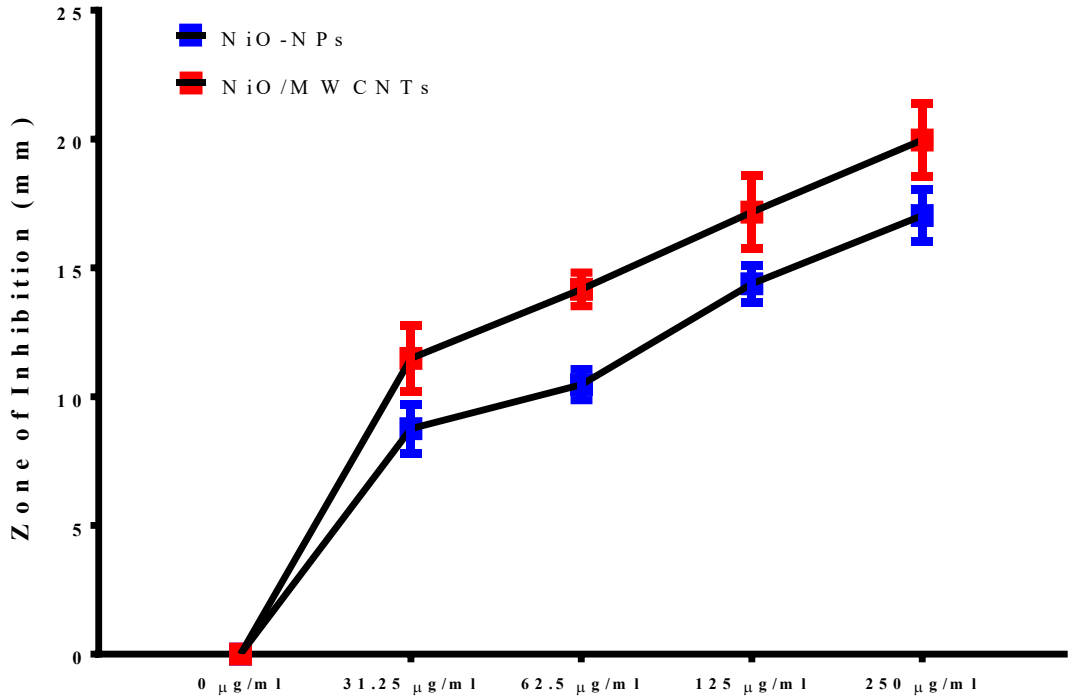

Figure 8 Antibacterial activity of NiO and NiO/MWCNTs nanocomposites against *S. aureus.*

The results shown in the Figure 9, indicate that the NiO/MWCNTs nanocomposite exhibits stronger antibacterial activity than pure NiO NPs**,** as evidenced by the larger inhibition zones at all tested concentrations (31.25–250 µg/ml) against *E. coli*. At 31.25 µg/ml, the inhibition zone for NiO/MWCNTs reached about 12 mm vs 9 mm for NiO-NPs. As the concentration increased 125, and 250 µg/ml, the inhibition zones for the nanocomposite increased to approximately 19 mm, and 22 mm, respectively, smaller zones 16 mm and 17 mm for NiONPs. These findings reveal that incorporating MWCNTs significantly enhances the antibacterial performance of NiO.

This enhancement can be related to several synergistic suggestion including: MWCNTs provide a large specific surface area improving dispersion of NiO nanoparticles and increasing the contact area with bacterial cells; the nanotubes can also physically damage membranes through a needle-like; and their high electrical conductivity may facilitate electron transfer reactions that promote ROS generation. Stronger antibacterial activity results from all of these consequences, which intensify oxidative stress and membrane disruption. These findings are consistent with widely reported nanomaterial antibacterial mechanisms reported in nanomedicine studies, in which metal oxide nanoparticles in combination with carbon nanostructures show increased bactericidal activity because of more powerful cell-surface interactions, enhanced particle stable state, and enhanced synergistic generation of ROS [40, 41]. As a result, NiO/MWCNT nanocomposites show better antibacterial activity than NiO nanoparticles alone, especially at higher concentrations, which makes them attractive options for biomedical and antimicrobial coatings. Taken together, these effects intensify oxidative stress and membrane disruption, resulting in greater antibacterial efficiency of the NiO/MWCNTs nanocomposite against *E. coli* compared with NiO alone.

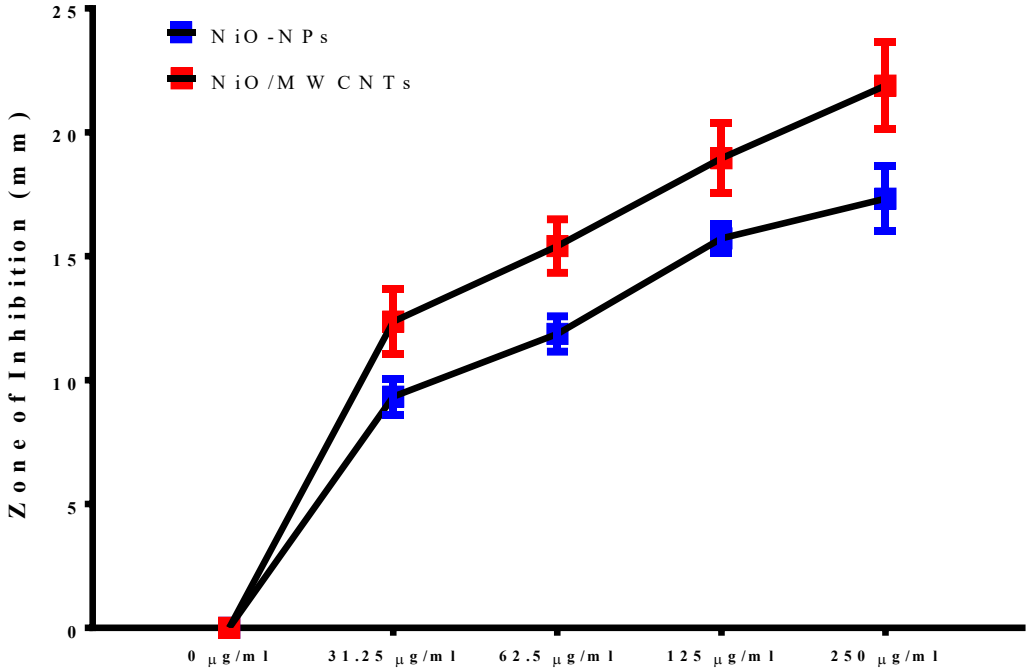

Figure 9 The antibacterial activity of NiO and NiO/MWCNTs nanocomposites against *E. coli.*

3.7 The cytotoxicity of prepared NiO and NiO/MWCNTs

By using cancer cells type A549 as a model lung cancer, the resulted nanoparticles NiO-NPs and NiO/MWCNTs are treated with these cells to investigate the determine how nanoparticles interact with human cells at the molecular and cellular levels to inhibit growth inhibition and proliferation. As shown in Figure 10, the cytotoxicity influence of NiO NPa and NiO/MWCNTs against A549 cells at lower concentrations (12.5 µg/ml and 25 µg/ml), reveal low cytotoxicity about (15% for NiO vs 22% for nanocomposites), and at 25 µg/ml the cytotoxicity is about (38% for NiO vs 50% nanocomposites), suggesting that these concentrations are not high enough to cause substantial damage. As the higher concentrations (50 µg/ml and 100 µg/ml), the cytotoxicity rises to about (38% and 63% for NiO vs 59% and 74% of NiO/MWCNTs) significantly these findings indicating that at higher doses, the nanocomposites is significantly disrupt the cells integrity due to the combined effects of membrane damage from MWCNTs and oxidative stress from NiO. These findings reveal the highest cytotoxicity of nanocomposites, due to the synergistic effects between MWCNTs membrane-disrupting properties and NiO oxidative stress generation leading to increased ROS production and activation of apoptotic pathways. As a result of this study suggested that NiO and nanocomposites at higher doses caused cell death. Moreover, the results reveal inside the cells, the NiO component can generate ROS, leading to oxidative stress. MWCNTs may also exacerbate this process by creating physical interactions with the cell membrane, allowing more ROS to penetrate the cells and causing further damage. Previous studies demonstrated the ability NiO and MWCNTs to destroy cancer cells.

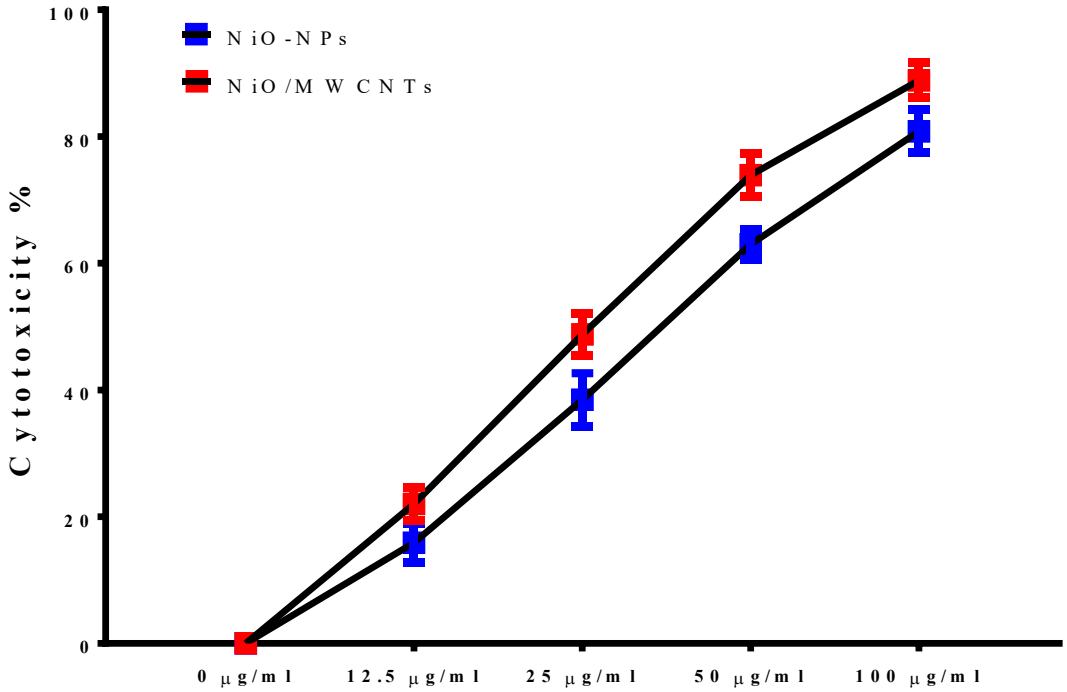

Figure 10 The Anti-cancer activity of NiO NPs and NiO/MWCNTs against A549 cells.

3.7 NiO/MWCNTs induces ROS generation in A549 cells

Figure 11 (a,b,c) represents intercellular reactive oxygen species (ROS) generation in A549 colon cancer cells after treated NiO and NiO/MWCNTs nanocomposites, analyzed by DCFDA 2,7-dichloroflurescin diacetate) fluorescence assay. In state of control untreated A549 cells, the fluorescence intensity is minimal; indicating normal ROS levels consistent with healthy cellular metabolism and no oxidative stress is detected as shown in Figure 11 a. A significant shift toward higher DCF fluorescence intensity is observed in Figure 11 b and c after treated with NiO and nanocomposites compared to control cells. The increasing of ROS levels is seen in A549 cells that had been treated with NiO and nanocomposites. This enhanced ROS production can lead to oxidative damage to proteins, lipids and DNA, initiating apoptotic. When the lung cancer cells are treated with nanocomposites, the outcomes revealed the levels of ROS is enhanced as shown in Figure 11c.

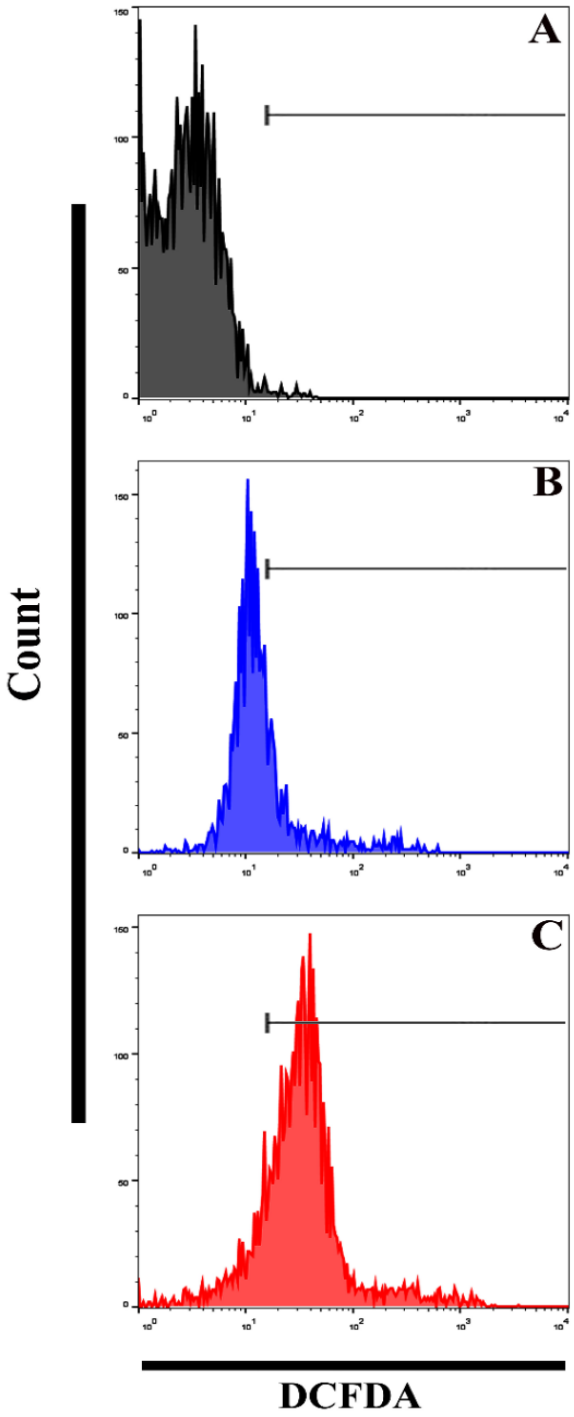

Figure 11 ROS generation in A549 cells using flow cytometry assay. A) Control untreated A549 cells, B) treated NiO NPs, C) treated NiO/MWCNTs.

The fluorescence intensity resulting from ROS is found to be higher after treated with nanocomposites as compared to control untreated cells. These findings confirm the large surface area of MWCNts that improve cellular uptake of nanocomposites and strong catalytic ROS-generating activity of NiO. Moreover, this combination leads to intracellular oxidative stress, which is consistent with the high apoptosis percentage seen in Annexin V assay.

4. CONCLUSIONS

In this study, the NiO and NiO/MWCNTs nanocomposites at molar ration 1:1 of NiO:MWCNTs were effectively synthesized using Sol-Gel method. The characterization results reveal that NiO exhibited face-centered cubic phase and the appearance of additional peaks of MWCNTs indicates that MWCNTs retain their graphic structure within the nanocomposites and small amount of MWCNTs had little effect on the morphology, optical and composition of NiO. In FE-SEM the MWCNTs appear as elongated tubular structures that form a continuous scaffold, effectively separating NiO domains and limiting direct particle–particle contact which result in agglomeration was suppressed, leading to a more porous and loosely packed architecture. In UV-vis analysis, the notable reduction of the band gap was attributed to the strong interfacial interaction between NiO_3 nanoparticles and MWCNTs, leading to the formation of Ni-O-C bonds, as confirmed by PL, FTIR and Raman analysis. Overall, these findings suggest that NiO/ MWCNTs nanocomposites at specific molar ratio 1:1 NiO:MWCNTs exhibit superior anticancer potential through the induction of apoptosis, primarily facilitated by ROS-dependent pathways. The synergistic interaction between the NiO and MWCNTs nanoparticles enhances the therapeutic efficacy while maintaining good dispersion and cellular interaction properties. Besides, the fact that NiO/MWCNTs nanocomposite at specific molar ratio 1:1 of NiO:MWCNTs shows higher toxicity than NiO NPs reveals that the combination of MWCNTs and NiO NPs enhance their biological activity, potentially through mechanism such as increased cellular uptake and ROS.

References

[1] K. Kaviyarasu, J. Kennedy, M. Maaza, B. Siddhardha, G. Sekaran, Ceram. Int. 49 (2023) 27230. https://doi.org/10.1016/j.ceramint.2023.05.273
[2] Y. Verma, G. Sharma, J. Iqbal, M. Naushad, C.W. Lai, A. Kumar, P. Dhiman, A. Mudhoo, Mater. Today Sustain. 28 (2024) 101041.https://doi.org/10.1016/j.mtsust.2024.101041
[3] A. Hamandi, J. Biomed. Photonics Eng. 7 (2021) 030405. https://doi.org/10.18287/JBPE21.07.030405
[4] S. Hussain, A. Aslam, A. Tajammal, F. Othman, Z. Mustafa, A.M. Alsuhaibani, M.S. Refat, M. Shahid, M. Sagir, Z.A. Zakaria, ACS Omega 9 (2024) 35408. https://doi.org/10.1021/acsomega.4c01328
[5] N.M. Omar, M.H. Othman, Z.S. Tai, J.Y. Heng, T.A. Kurniawan, M.H. Puteh, S.A. Bakar, J.Jaafar, M.A. Rahman, J. Mater. Sci. 59 (2024) 19450. https://doi.org/10.1007/s10853-024-09321-0
[6] S. Darvishi, A.A. Ensafi, K.Z. Mousaabadi, Sci. Rep. 14 (2024) 7576. https://doi.org/10.1038/s41598-024-07576-2
[7] A. Kiran, S. Hussain, I. Ahmad, M. Imran, M. Saqib, B. Parveen, K.S. Munawar, W. Mnif, M. Al Huwayz, N. Alwadai, M. Iqbal, Heliyon 10 (2024) e25984. https://doi.org/10.1016/j.heliyon.2024.e25984
[8] E. Piatti, D. Torsello, F. Breccia, T. Tamegai, G. Ghigo, D. Daghero, Nanomaterials 14 (2024) 1319. https://doi.org/10.3390/nano14151319

Exp. Theo. NANOTECHNOLOGY 10 (2026) 1255-1274
[9] G. Matyszczak, K. Głuc, K. Krawczyk, Catalysts 16 (2026) 208. https://doi.org/10.3390/catal16030208
[10] O.C. Pore, A.V. Fulari, N.B. Velhal, V.G. Parale, H.H. Park, R.V. Shejwal, V.J. Fulari, G.M. Lohar, Mater. Sci. Semicond. Process. 134 (2021) 105980. https://doi.org/10.1016/j.mssp.2021.105980
[11] A.C. Hamandi, R.V. Skidanov, N.A. Firsov, P.V. Boriskin, V.V. Podlipnov, A.R. Makarov, A.V. Nikonorov, in: 2022 VIII Int. Conf. Inf. Technol. Nanotechnol. (ITNT), IEEE, 2022 https://doi.org/10.1109/ITNT55410.2022.9848617
[12] Z.R. Rahoomi, D.S. Ahmed, M.S. Jabir, H. Samir, A.A. Swelum, PLoS One 19 (2024) e0309389. https://doi.org/10.1371/journal.pone.0309389
[13] K.A. Obaid, A.A. Imarah, H.M. Khalfa, G.M. Sulaiman, M.S. Jabir, M.K. Mohammed, et al., J. Trace Elem. Med. Biol. 86 (2024) 127569. https://doi.org/10.1016/j.jtemb.2024.127569
[14] S.D. Al-Algawi, R.T. Rasheed, S.Z. Tareq, Eng. Technol. J. B 33 (2015) 984.
[15] V.G. Kessler, G.A. Seisenbaeva, J. Sol-Gel Sci. Technol. 107 (2023) 190. https://doi.org/10.1007/s10971-023-06120-y
[16] A.C. Nkele, A. Alshoaibi, F.D. Matthew, C. Awada, S. Islam, F.I. Ezema, J. Sol-Gel Sci. Technol. 114 (2025) 874. https://doi.org/10.1007/s10971-025-06701-2
[17] Z.R. Rhoomi, D.S. Ahmed, M.S. Jabir, B. Balasubramanian, M.A. Al-Garadi, A.A. Swelum, ACS Omega 8 (2023) 37147. https://doi.org/10.1021/acsomega.3c04761
[18] A. Hamandi, H.H. Abdulghani, R.F. Kadhim, M.H. Amin, S.M. Majeed, D.S. Ahmed, Experimental and Theoretical NANOTECHNOLOGY 10 (2026) 1013. https://doi.org/10.56053/10.S.1013
[19] M. Alhujaily, M.S. Jabir, U.M. Nayef, T.M. Rashid, G.M. Sulaiman, K.A. Khalil, et al., Metals 13 (2023) 735. https://doi.org/10.3390/met13040735
[20] A. Adiba, V. Pandey, S. Munjal, T. Ahmad, AIP Conf. Proc. 2270 (2020) 110011. https://doi.org/10.1063/5.0028010
[21] Haitham Mohammed Ibrahim Al-Zuhairi, Iqbal alshalal, Hind H. Abbood, M. Al Nuaimi, Experimental and Theoretical NANOTECHNOLOGY, 10 (2026) 855 https://doi.org/10.56053/10.S.855
[22] H.M. Kotb, M.M. Ahmad, S.A. Ansari, T.S. Kayed, A. Alshoaibi, Molecules 27 (2022) 779. https://doi.org/10.3390/molecules27030779
[23] Y. Tanaka, Am. J. Mater. Eng. 3 (2022) 8.
[24] S. Senthilkumar, K. Revathi, R. Venkatesh, E. Sivaprakash, Int. J. Metalcast. 18 (2024) 1465. https://doi.org/10.1007/s40962-023-01083-2
[25] H.M. Ahmed, M.H. Al-Ameri, A.A. Alkhafaji, M.S. Jabir, B.A. Hasoon, D.S. Ahmed, (2026) 1. https://doi.org/10.1007/s44174-026-00644-x
[26] S.J.P. Begum, S. Pratibha, J.M. Rawat, D. Venugopal, P. Sahu, A. Gowda, K.A. Qureshi, M. Jaremko, Pharmaceuticals 15 (2022) 455. https://doi.org/10.3390/ph15040455
[27] M. Mohamed, E.K. Jaradat, A.S. Alshammari, A. Sedky, Sci. Rep. 15 (2025) 40353. https://doi.org/10.1038/s41598-025-40353-0
[28] Alyaa Hussain, Ibtihal A. Mahmood, Hussein A. Hussein, Experimental and Theoretical NANOTECHNOLOGY, 10, 907-924. https://doi.org/10.56053/10.S.907
[29] C. Suryanarayana, T. Klassen, E. Ivanov, J. Mater. Sci. 46 (2011) 6301. https://doi.org/10.1007/s10853-011-5529-2
[30] X. Chen, Y. Lou, S. Dayal, X. Qiu, R. Krolicki, C. Burda, C. Zhao, J. Becker, J. Nanosci. Nanotechnol. 5 (2005) 1408. https://doi.org/10.1166/jnn.2005.182
[31] M.H. Al-Ameri, A.L. Abed, S.M. Majeed, H.M. Ahmed, A.A. Alkhafaji, A. Malik, T.A. Kurniawan, M.A. Said, S. Ali, I. Ali, Inorg. Chem. Commun. (2026) 116861. https://doi.org/10.1016/j.inoche.2026.116861

[32] A.A. Mohd Raub, R. Bahru, M.A. Mohamed, R. Latif, M.A. Mohammad Haniff, K. Simarani, J. Yunas, Nanotechnology 35 (2024) 242004. https://doi.org/10.1088/1361-6528/ad3f2c
[33] W. Yan, X. Wang, D.W. Pang, J. Cai, Nano Res. 18 (2025) 94907158. https://doi.org/10.1007/s12274-025-7158-x
[34] M.S. Alqahtani, F.A. Alharthi, S.A. Alotaibi, R.M. Alanazi, J. Mater. Sci. Mater. Electron. 34 (2023) 14215. https://doi.org/10.1007/s10854-023-10345-2
[35] L. Kang, C. Yang, Adv. Eng. Mater. 21 (2019) 1801359. https://doi.org/10.1002/adem.201801359
[36] Q. Wang, B. Yu, B. Yang, X. Zhang, G. Yu, Z. Wang, H. Qin, Y. Ma, Nanomaterials 15 (2025) 266. https://doi.org/10.3390/nano15040266
[37]
[38] T. Zhang, W. Liu, B. Dong, Y. Wu, W. Yang, Y. Zhao, Y. Fan, L. Chen, Mater. Chem. Phys. 276 (2022) 125365. https://doi.org/10.1016/j.matchemphys.2021.125365
[39] J. Wei, Q. Wang, M. He, S. Li, Y. Zhang, Y. Yang, S. Luo, L. Fu, X. Wang, T. Yang, Appl. Surf. Sci. 612 (2023) 155726. https://doi.org/10.1016/j.apsusc.2022.155726
[40] M.S. Jabir, M.K.A. Mohammed, S. Albukhaty, D.S. Ahmed, A. Syed, A.M. Elgorban, R. Eswaramoorthy, H.M. Al-Kuraishy, A.I. Al-Gareeb, S. Ghotekar, S.F. Jawad, M.A. Najm, Nanotechnol. Rev. 12 (2023) 20230127. https://doi.org/10.1515/ntrev-2023-0127
[41] S.M. Al-Jawad, Z.S. Shakir, D.S. Ahmed, Eur. Phys. J. Appl. Phys. 96 (2021) 21201. https://doi.org/10.1051/epjap/202121201